ChemComm

COMMUNICATION

View Article Online
View Journal | View Issue

Cite this: *Chem. Commun.*, 2018, **54**, 12594

Received 17th September 2018,
Accepted 12th October 2018

DOI: 10.1039/c8cc07508e

rsc.li/chemcomm

Homogeneous enzyme-free and entropy-driven isothermal fluorescent assay for nucleic acids based on a dual-signal output amplification strategy†

Erhu Xiong, Deshuai Zhen and Ling Jiang *

Herein, we developed a homogeneous enzyme-free, ultrasensitive and isothermal fluorescent biosensor for nucleic acid detection with dual-signal output to enhance the reaction rate and sensitivity by combining an entropy-driven catalysis strategy with a catalytic hairpin assembly reaction.

Nucleic acid-based biosensors are of crucial importance in modern life sciences and have been extensively used for the detection of many biomarkers of disease and widely applied in many fields, such as gene therapy, medical analysis, and pathogen determination.[1,2] As one of the most important biomarkers, nucleic acids are related to the expression of genetic information in living organisms, so little changes in nucleic acid sequences can lead to remarkable biological and biomedical implications.[3,4] Therefore, the low abundance of mutants in nucleic acids necessitates some amplification strategies in most cases to achieve a sensitive signal output. As is well known, DNA amplification strategies have great potential in trace biomarker determination and disease diagnostics because of their excellent signal-amplifying capabilities. In recent years, considering the importance of nucleic acid analysis, many signal amplification techniques have been proposed, such as the polymerase chain reaction (PCR),[5] rolling circle amplification (RCA),[6] ligase chain reaction (LCR),[7,8] enzyme-assisted target recycling strategy,[9,10] loop-mediated isothermal amplification (LAMP)[11,12] and so on. Among these signal amplification techniques, PCR can be regarded as the most often used approach for DNA amplification, but it needs polymerase, complex thermocycling procedures and specialized equipment. However, the other signal amplification techniques are also enzyme-based methods. The involvement of enzymes may lead to non-specific reactions and increase the risk of false-positive signal outputs, and in some cases utilizing multiple sorts of enzymes can increase the assay cost and reduce the portability of target determination. In addition, most enzymes are highly sequence-specific and impressionable to the test environment, and enzymatic probe reactions require strict conditions (such as temperature, pH value, and salinity) to proceed, which may limit their extensive application.[13,14] Therefore, the exploration of isothermal and enzyme-free signal amplification strategies for ultrasensitive target detection is highly desired and advocated to improve the analytical performance.

Yurke *et al.* proposed a tweezer-like dynamic molecular machine which first involved a toehold-mediated strand displacement reaction.[15] When two single-stranded DNAs (ss-DNAs) share the same domain, they will bind to the complementary-stranded domain competitively and the shorter ss-DNA is displaced by the external introduction of longer ss-DNA through its hybridization with an overhang region (toehold domain) to trigger the strand displacement process.[16,17] In view of this principle, an enzyme-free signal amplification circuit based on catalytic hairpin assembly (CHA) has been constructed by Yin *et al.*,[18] using a ss-DNA as a catalyst to initiate two continuous toehold-mediated strand displacement reactions that assemble two hairpins into double-stranded products. In general, an ideal CHA reaction can amplify a signal 50 to 100-fold within a few hours.[19] Because of the high signal-to-noise ratio and programmability, CHA reaction has been extensively used for various analytical platforms and can be regarded as a new generation of transducers and signal amplifiers. In addition, in a milestone report in the area of DNA circuits, an entropy-driven catalysis (EDC) strategy was proposed by Zhang *et al.*, which was driven forward by the augmentation of entropy in the reaction system and formed a stable double-stranded complex, leading to an irreversible reaction.[20] Based on the EDC strategy, He *et al.* reported a mRNA-triggered, three-dimensional DNA amplifier which could be used in the interior of living cells.[21] Lv *et al.* developed a DNA amplification strategy without hairpins for the sensitive determination of nucleic acids.[22] Kim *et al.* and Yang *et al.* separately developed two different kinds of biosensor for protein assay based on aptamer/protein proximity binding and the EDC strategy.[23,24] Unfortunately, although these methods achieved their goals for target detection, there was only

State Key Laboratory of Chemo/Biosensing and Chemometrics, College of Chemistry and Chemical Engineering, Hunan University, Changsha, 410082, P. R. China. E-mail: ljiang630@163.com

† Electronic supplementary information (ESI) available. See DOI: 10.1039/c8cc07508e

one kind of signal amplification method and there were many by-products yielded in the biosensing system, which resulted in wasted DNA strands. Therefore, it is highly desirable to develop a more useful and efficient signal amplification strategy to directly improve the sensitivity of the DNA amplifier and make full use of the DNA strands in the biosensing system as well as to obtain excellent reliability and high signal output.

Considering the advantages of the CHA reaction and the EDC strategy, we herein reported a homogeneous enzyme-free, ultrasensitive and isothermal fluorescent biosensor for nucleic acid detection with dual-signal output by combining the EDC strategy (Cycle I) with the CHA reaction (Cycle II) (Scheme 1). With the existence of target DNA (T-DNA), the T-DNA could hybridize with the premade three-strand duplex (TD) through the toehold region (domain 7) to displace domain 6* of the output strand (OS) and initiate the EDC process, leading to the release of the OS used as an opener of fluorescent reporter I (FR I) and exposing a prelocked toehold region (domain 5) for hybridization with a fuel strand (FS). The hybridization between the FS and a substrate strand (SS) resulted in the release of T-DNA used for Cycle I and an auxiliary strand (AS) used as a trigger of the CHA reaction *via* the toehold region (domain 1) of hairpin 1 (H1), which avoided wasting the AS, and the newly exposed toehold region (domain 3*) of H1 could open hairpin 2 (H2) to form a H1/H2 duplex, which was used as an opener of fluorescent reporter II (FR II). In addition, FR I and FR II were made from two complementary linear oligonucleotide probes, one labeled with a donor fluorophore (FAM) and the other labeled with an acceptor quencher (IABkFQ). In the case of the duplex, the fluorophore FAM was quenched by IABkFQ due to the fluorescence resonance energy-transfer (FRET) effect, which is a distance-dependent process where energy from one fluorophore is transferred to another fluorophore if they are in close proximity (usually <6 nm). When FR I and FR II hybridized with the triggers, the double-stranded FR I and FR II would be dissociated, resulting in an increased distance between FAM and IABkFQ, thus a dual-signal fluorescence amplification was obtained based on the real-time signal outputs from FR I and FR II. In particular, the two FRs for signal output were introduced for the consumption of the products from Cycle I and Cycle II to push the equilibrium and significantly increase the analysis fold amplification for the improvement of reaction rate and sensitivity. Based on the proposed strategy, the developed fluorescent biosensor displayed a wide linear relationship in the range of 50 fM to 5 nM with a limit of detection (LOD) of 15.6 fM, Moreover, the biosensor avoided the involvement of any washing steps, thermocycling procedures and enzymes for target recycling amplification, which gave the fluorescent biosensor great potential for the convenient determination of nucleic acids in biomedical research and disease diagnostics.

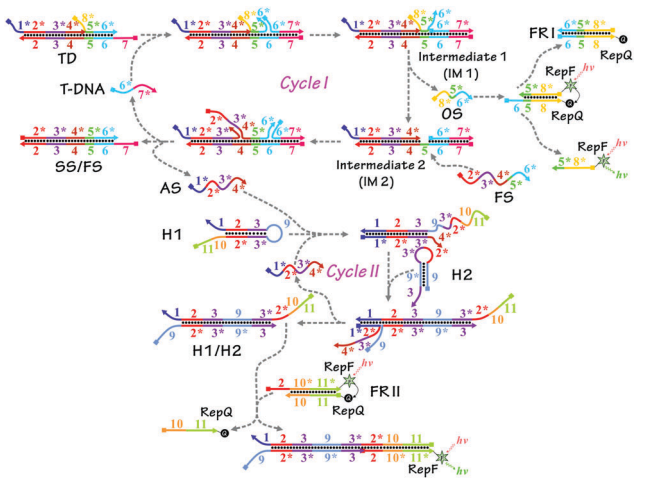

Scheme 1 Schematic illustration of the assay reaction mechanism.

The whole process of the EDC strategy is shown in Fig. 1A as a parameter-labeled reaction equation. The related thermodynamic theory is also calculated based on the Gibbs free energy equation,

$$\Delta G = \Delta H - T\Delta S \quad (1)$$

where ΔH stands for the change in system enthalpy, ΔS stands for the change in entropy, and T stands for the thermodynamic temperature. Because there is no change in the total number of base pairs of the reactants and products, $\Delta H \approx 0$. Thus, the reaction is driven forward thermodynamically by the entropic gain of the liberated molecules and the driving force, at any moment, is $T\Delta S$.

The final concentration of all species in the EDC system can be approximated. Based on the van't Hoff equation, the change of Gibbs free energy is given by

$$\Delta G = \Delta G^0_{OS} + \Delta G^0_{AS} + \Delta G^0_{SS/FS} - \Delta G^0_{TD} - \Delta G^0_{FS} + RT\ln Q \quad (2)$$

where Q stands for the reaction quotient, which is related to standard conditions ($Q = \{([OS]/c^0)([AS]/c^0)([SS/FS]/c^0)/([TD]/c^0)([FS]/c^0)\}$), R stands for the gas constant (8.314 J mol^{-1} K^{-1}), T stands for the thermodynamic temperature with units of K

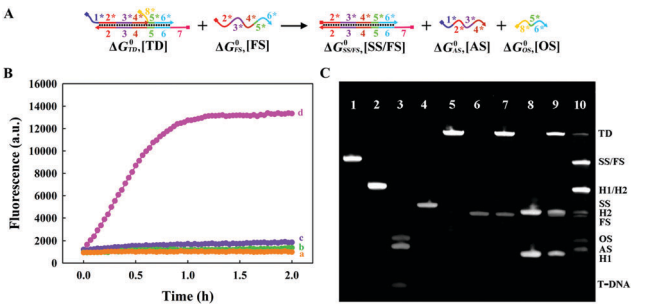

Fig. 1 (A) Reaction equation of the EDC strategy with thermodynamic parameters. (B) Fluorescence responses under different experimental conditions. (a) Cycle I with FR I in the absence of T-DNA, (b) Cycle II with FR II in the absence of T-DNA, (c) Cycle I with FR I and Cycle II with FR II in the absence of T-DNA, and (d) Cycle I with FR I and Cycle II with FR II in the presence of 5 nM T-DNA; (C) 10% native PAGE to analyse the biosensing system. Lane 1: 5 μM annealed product of SS/FS; lane 2: 5 μM annealed product of the H1/H2 duplex; lane 3: 5 μM T-DNA + AS + OS; lane 4: 5 μM SS; lane 5: 5 μM TD; lane 6: 5 μM FS; lane 7: 5 μM TD + FS; lane 8: 5 μM H1 + H2; lane 9: 2.5 μM TD, 3 μM FS, 2.5 μM H1, and 5 μM H2; lane 10: 2.5 μM TD, 3 μM FS, 2.5 μM H1, 5 μM H2, and 10 nM T-DNA.

and ΔG^0_X stands for the standard free energy of species X with units of kcal mol^{-1} under standard conditions (TAE/Mg^{2+} buffer with 12.5 mM $MgCl_2$, pH 8.0, and c^0 = 1 M), which can be calculated by the use of some free software, for instance, Mfold or NUPACK,[25] giving

$$\Delta G^0_{OS} + \Delta G^0_{AS} + \Delta G^0_{SS/FS} - \Delta G^0_{TD} - \Delta G^0_{FS} = -0.57 \text{ kcal mol}^{-1} \quad (3)$$

When the EDC system reaches equilibrium, which means ΔG = 0, the value of Q can be calculated as 2.52 based on eqn (2) and (3).

Presuming that the initial concentrations of TD and FS are both 100 nM, and the final concentration of OS is x nM, the equation can be written as follows:

$$\frac{(10^{-9}x)^3}{[10^{-9}(100-x)]^2} = 2.52$$

According to the bisection method, x can be evaluated to be in the range from 99.9 to 99.99 nM, which could lead to a potential systemic conversion of more than 99.9%, regardless of the reaction time.

The feasibility of the developed biosensor was first verified. As displayed in Fig. 1B, in the absence of T-DNA, the EDC strategy (curve a) and the CHA reaction (curve b) displayed low background fluorescence signal. Even though there was a small increase in the background fluorescence signal, it was still negligible for the entire biosensing system in the absence of T-DNA (curve c). However, in the presence of 5 nM T-DNA, the fluorescence signal increased significantly (curve d). As displayed in Fig. 1C, 10% native PAGE was used to further verify the feasibility of the developed biosensing system. Compared with lane 9 which was just in the presence of TD, FS, H1 and H2 without T-DNA, two bright bands with significantly decreased migration shift were observed (lane 10). Meanwhile, the bands of TD, FS, H1 and H2 almost disappeared and the new bands of OS and AS appeared, which could be because of the initiated strand displacement between TD and FS by T-DNA (EDC process) and the CHA reaction, but the added T-DNA was only 10 nM so it could not be seen clearly. In addition, lanes 1–8 were used as markers or references. Thus, the PAGE results were in strong accordance with the results of the fluorescence signals, indicating that the feasibility was satisfactory.

Furthermore, to image the assay visually and verify the feasibility once again, the biosensing system was also used on the microparticle surface. In the CHA reaction, as shown in Fig. S1A (ESI†), in brief, two hairpins (H1 and H2) were kinetically trapped, but in the presence of the catalyst (AS), they could initiate the strand displacement process that led to the formation of a double-stranded duplex (H1/H2) and the release of AS which could then take part in the downstream reaction cycles on the microparticle surface. The formation of H1/H2 duplex was used as a fuel to drive the movement of the walker (AS), resulting in increasing microparticle fluorescence. In order to examine the autonomy and processivity of the DNA walking, the microparticle fluorescence was imaged at different time points of the 60 min operation (Fig. S1B, ESI†). In the absence of T-DNA, the EDC process could not occur and AS could not be released, so there was no fluorescence observed on the microparticle. In the presence of 5 nM T-DNA, the fluorescence increased steadily over the operating time (10 min, 30 min, and 60 min), indicating that the DNA walked along the microparticle surface autonomously and continuously, and the proposed strategy was feasible.

The EDC strategy translated a molecular input (T-DNA, shown in Scheme 1) into an amplified amount of two different single-stranded output sequences (OS and AS). As shown in Fig. 2, three cases were designed to interact with OS or AS alone, or both OS and AS. OS would interact with FR I to generate a fluorescence signal (Fig. 2A, Case 1), and AS would initiate the CHA reaction, and then interact with FR II to generate a fluorescence signal (Fig. 2B, Case 2). Thus, interacting with these strands (OS or AS) would have an obvious influence on the entire biosensing system. However, more importantly, interacting with both OS and AS generated the largest fluorescence signal (Fig. 2C, Case 3, dual-signal output strategy). The combination of the fluorescence signals of the three cases in the absence or presence of T-DNA is displayed in Fig. 2D. The fluorescence signals of all three cases were very small without T-DNA. In the presence of 10 nM T-DNA, based on Fig. 2D, the influence of the dual-signal output on the entire biosensing system could be divided into two aspects: signal generation and initial reaction rate. Compared with Cases 1 and 2, Case 3 caused a ~2-fold enhancement in signal generation, which would greatly improve the sensitivity of the biosensing system. In addition, although the three cases reached the plateau almost at the same time, the initial reaction rate of Case 3 was much faster than that of Case 1 and 2 alone, indicating that the dual-signal output strategy could accelerate the signal generation significantly.

To investigate the sensitivity and potential applications of the developed fluorescent biosensor with dual-signal output by combining the EDC strategy and the CHA reaction, various concentrations of T-DNA were assayed. As displayed in Fig. 3A,

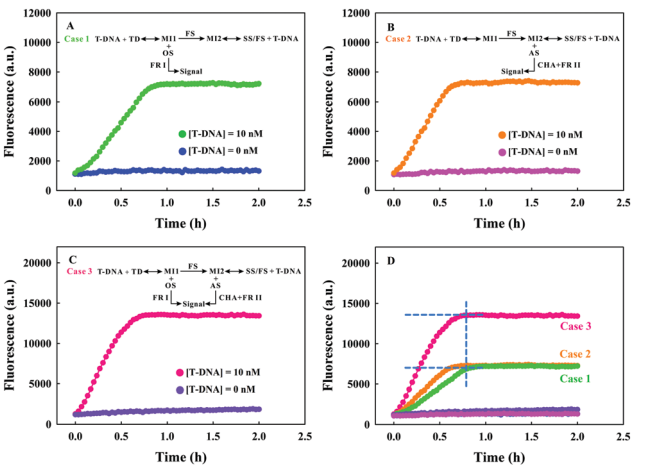

Fig. 2 Three different reaction cases in the absence or presence of 10 nM T-DNA. (A) Fluorescence signal generation by OS alone; (B) fluorescence signal generation by AS alone; (C) fluorescence signal generation by both OS and AS; (D) combination of the fluorescence signals of the three cases.

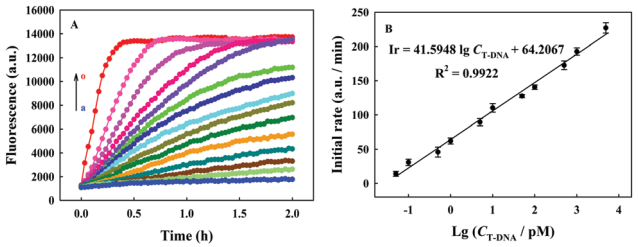

Fig. 3 (A) Fluorescence responses for the assay of different T-DNA concentrations. The concentrations are (from a to o) 0, 10 fM, 50 fM, 100 fM, 500 fM, 1 pM, 5 pM, 10 pM, 50 pM, 100 pM, 500 pM, 1 nM, 5 nM, 10 nM, and 20 nM; (B) linear relationship between the initial rate and the logarithm of T-DNA concentrations. Error bars represent standard deviations of three separate assays.

the fluorescence signals enhanced with the increase of T-DNA concentrations in the range of 10 fM to 20 nM. Moreover, it was noted that the initial rate was linear with the logarithm of T-DNA concentration in the range of 50 fM to 5 nM (Fig. 3B), and the linear regression equation was Ir = 41.5948 lg $C_{T\text{-}DNA}$ + 64.2067 (R^2 = 0.9922, Ir was the initial rate) with a LOD of 15.6 fM (S/N = 3), which meant that the analytical performance of the proposed biosensing system was superior to that of some existing T-DNA analytical methods and isothermal nucleic acid amplification techniques (Tables S2 and S3, ESI†).

Specificity is a critical factor for evaluating the success of the proposed biosensing system. Thus, the specificity was evaluated by measuring the fluorescence responses to four different sorts of DNA sequence. The results shown in Fig. S2 (ESI†) clearly indicated that the proposed fluorescent biosensor possessed excellent specificity for the TDNA assay.

To study the applicability of the developed fluorescent biosensor for real samples, T-DNA with various concentrations (5 pM, 10 pM, 50 pM, 100 pM) was added in 10-fold diluted serum samples, which were diluted with the TAE/Mg^{2+} buffer. As shown in Table S4 (ESI†), the recoveries for the added T-DNA were 99.2%, 101.3%, 98.74%, and 102.67%, respectively, which was satisfactory for sensitive assays performed in complex real samples.

In summary, a homogeneous enzyme-free, ultrasensitive and isothermal fluorescent biosensor for T-DNA determination with dual-signal output by combining the EDC strategy and the CHA reaction was developed, which led to an amplified signal to enhance the reaction rate and sensitivity. The proposed fluorescent biosensor exhibited three attractive features. First, the developed homogeneous method is performed without any enzymes, washing steps, or precise temperature cycling. Second, the fluorescent biosensor with dual-signal output has excellent analytical performance with a LOD of 15.6 fM, and shows outstanding recognition toward mismatched DNA strands. Third, the proposed fluorescent biosensor provides a potential universal platform for the determination of other nucleic acids. With these advantages, the method will have great promise for applications in the fields of bioanalysis, clinical biomedicine, and disease diagnostics.

This work was supported by the NSFC (21475035, 21727810), the Foundation for Innovative Research Groups of NSFC (21521063) and the China Scholarship Council (201606130011).

Conflicts of interest

There are no conflicts to declare.

Notes and references

1 A. Furst, S. Landefeld, M. G. Hill and J. K. Barton, *J. Am. Chem. Soc.*, 2013, **135**, 19099–19102.
2 D. J. Lockhart and E. A. Winzeler, *Nature*, 2000, **405**, 827–836.
3 J. H. Chen, J. Zhang, Y. Guo, J. Li, F. F. Fu, H. H. Yang and G. N. Chen, *Chem. Commun.*, 2011, **47**, 8004–8006.
4 E. H. Xiong, Z. Z. Li, X. H. Zhang, J. W. Zhou, X. X. Yan, Y. Q. Liu and J. H. Chen, *Anal. Chem.*, 2017, **89**, 8830–8835.
5 R. K. Saiki, S. Scharf, F. Faloona, K. B. Mullis, G. T. Horn, H. A. Erlich and N. Arnheim, *Science*, 1985, **230**, 1350–1354.
6 P. He, W. P. Qiao, L. J. Liu and S. S. Zhang, *Chem. Commun.*, 2014, **50**, 10718–10721.
7 F. Barany, *Proc. Natl. Acad. Sci. U. S. A.*, 1991, **88**, 189–193.
8 E. J. Wee, M. J. Shiddiky, M. A. Brown and M. Trau, *Chem. Commun.*, 2012, **48**, 12014–12016.
9 E. H. Xiong, X. X. Yan, X. H. Zhang, Y. Q. Liu, J. W. Zhou and J. H. Chen, *Biosens. Bioelectron.*, 2017, **87**, 732–736.
10 E. H. Xiong, X. H. Zhang, Y. Q. Liu, J. W. Zhou, P. Yu, X. Y. Li and J. H. Chen, *Anal. Chem.*, 2015, **87**, 7291–7296.
11 Y. S. Jiang, S. Bhadra, B. Li, Y. R. Wu, J. N. Milligan and A. D. Ellington, *Anal. Chem.*, 2015, **87**, 3314–3320.
12 B. L. Li, X. Chen and A. D. Ellington, *Anal. Chem.*, 2012, **84**, 8371–8377.
13 K. Shi, B. T. Dou, C. Y. Yang, Y. Q. Chai, R. Yuan and Y. Xiang, *Anal. Chem.*, 2015, **87**, 8578–8583.
14 D. Yin, Y. Y. Tao, L. Tang, W. Li, Z. Zhang, J. L. Li and G. M. Xie, *Microchim. Acta*, 2017, **184**, 3721–3728.
15 B. Yurke, A. J. Turberfield, A. P. Mills Jr, F. C. Simmel and J. L. Neumann, *Nature*, 2000, **406**, 605–608.
16 S. X. Chen, D. Y. Zhang and G. Seelig, *Nat. Chem.*, 2013, **5**, 782–789.
17 D. Y. Zhang and E. Winfree, *J. Am. Chem. Soc.*, 2009, **131**, 17303–17314.
18 P. Yin, H. M. Choi, C. R. Calvert and N. A. Pierce, *Nature*, 2008, **451**, 318–322.
19 Z. T. Zhu, Y. D. Tang, Y. S. Jiang, S. Bhadra, Y. Du, A. D. Ellington and B. L. Li, *Sci. Rep.*, 2016, **6**, 36605.
20 D. Y. Zhang, A. J. Turberfield, B. Yurke and E. Winfree, *Science*, 2007, **318**, 1121–1125.
21 L. He, D. Q. Lu, H. Liang, S. T. Xie, X. B. Zhang, Q. L. Liu, Q. Yuan and W. H. Tan, *J. Am. Chem. Soc.*, 2017, **140**, 258–263.
22 Y. F. Lv, L. Cui, R. Z. Peng, Z. L. Zhao, L. P. Qiu, H. P. Chen, C. Jin, X. B. Zhang and W. H. Tan, *Anal. Chem.*, 2015, **87**, 11714–11720.
23 D. Kim, O. B. Garner, A. Ozcan and D. D. Carlo, *ACS Nano*, 2016, **10**, 7467–7475.
24 J. M. Yang, B. T. Dou, R. Yuan and Y. Xiang, *Anal. Chem.*, 2017, **89**, 5138–5143.
25 J. N. Zadeh, C. D. Steenberg, J. S. Bois, B. R. Wolfe, M. B. Pierce, A. R. Khan, R. M. Dirks and N. A. Pierce, *J. Comput. Chem.*, 2011, **32**, 170–173.